Impact of Toroidal Rotation and Safety Factor on Ion Turbulent Transport in Tokamaks

Y. Idomura[1], S. Jolliet[1], M. Yoshida[2], and H. Urano[2]
[1] Japan Atomic Energy Agency, Higashi-Ueno 6-9-3, Taitou, 110-0015 Tokyo
[2] Japan Atomic Energy Agency, Mukoyama 801-1, Naka, Ibaraki, 311-0193, Japan

E-mail contact of main author: idomura.yasuhiro@jaea.go.jp

Abstract. An impact of the toroidal rotation and the safety factor q on the ion temperature gradient driven (ITG) turbulence is studied using a global gyrokinetic toroidal full-f five dimensional Eulerian code GT5D [Idomura et al., Nucl. Fusion 49, 065029]. In the rotation scan numerical experiments, the radial electric field E_r profile is changed depending on the toroidal rotation. Although local transport levels are affected by the E_r profile, global transport properties are not changed, when the magnitudes of its shearing rate are in similar levels on average. In the q scan numerical experiments, turbulent transport is significantly enhanced at higher q. It is found that the stabilizing effect of E_r shear on liner ITG modes becomes less effective at higher q. Both the ion heat transport and the non-diffusive momentum transport are enhanced. The former leads to lower ion temperature gradient, while the latter produces larger inward momentum flux and co-current spontaneous rotation in the plasma core.

1 Introduction

The ion temperature gradient driven (ITG) turbulence is considered as a main candidate to explain the ion heat transport in tokamak experiments. H-mode plasmas often show stiff ion temperature T_i profiles with globally constant gradient parameters R_0/L_{ti} or exponential profiles [1]. Since this feature dictates the total performance of H-mode plasmas once the pedestal temperature is given, the understanding of ion heat transport mechanisms leading to the profile stiffness is an important issue. In the experiment, this issue was addressed in recent dedicated experiments on JT-60U [1] and JET [2]. The former showed very small changes in R_0/L_{ti} among plasmas with co-current, balance, and counter-current neutral beam injections (NBIs). On the other hand, the latter showed a significant change of R_0/L_{ti} between plasmas with co-current and counter-current NBIs (or high and low toroidal rotation). Therefore, an impact of the toroidal rotation (and its shear) on the ion heat transport and the stiffness of T_i profile is a puzzling issue. In the theory, effects of the toroidal rotation shear can be decomposed into a stabilizing effect of the $E \times B$ shear and a destabilizing effect of the parallel velocity shear [3]. The net effect is determined by a delicate balance between them, which often cancel with each other [4]. However, most of former studies did not take account of poloidal rotation, profile shear (so-called ω^*-shear), and so-called intrinsic rotation in a force balance relation, which are typically small flows but their shear may not be negligible.

Another important ingredient dictating confinement properties is the plasma current I_p. The I_p dependence of the energy confinement was universally observed in H-mode plasmas on many tokamaks, where the core stored energy is proportional to $I_p^{0.9}$ [5]. In addition, recent momentum transport studies shed a new light on the momentum transport by showing the I_p dependence of intrinsic toroidal rotation, which is inversely proportional to I_p [6]. The I_p dependence or the safety factor q dependence of turbulent heat transport was explained based on quasi-linear models with the q dependence of the radial wave number $k_r \propto q^{-1/2}$ [7] and with the downshift of turbulent spectrum [3]. In

recent works, it was also pointed out that geodesic acoustic mode (GAM) activities play an important role in interfering the turbulence suppression due to steady zonal flows [8]. However, in most of existing works, the q dependence of the momentum transport has not been addressed, and theories on the latter issue are not matured.

In order to address the above issues, a comprehensive transport simulation involving both turbulent heat and momentum transport in a consistent manner is required. In this work, we perform the rotation scan and q scan numerical experiments using a global Gyrokinetic Toroidal full-f 5D Eulerian code (GT5D) [9, 10]. In GT5D, we solve the equilibrium distribution f_0 and the turbulent perturbation δf simultaneously, based on the same first principles, and the ion temperature T_i, the parallel flow $U_\parallel$, and the radial electric field E_r are evolved self-consistently under fixed momentum and power inputs as in the experiment. Here, mean E_r profiles are determined by the neoclassical physics, while micro- or meso-scale structures are produced by turbulent fluctuations. In Ref. [10], source driven ITG turbulence in normal shear tokamaks with an on-axis heating condition was studied, and a qualitative validation of GT5D was shown through comprehensive observations of main features of the ion turbulent transport such as the stiffness of T_i profiles, an intermittency of heat transport, and non-diffusive momentum transport leading to intrinsic rotation. In particular, stiff T_i profiles were reproduced for the first time based on the gyrokinetic theory. Therefore, a numerical experiment using GT5D is useful as a testing environment to explore comprehensive transport properties involving turbulent heat and momentum transport. In order to enable the rotation scan and q scan numerical experiments, GT5D has been extended including a momentum source model and a field-aligned gyrokinetic Poisson solver [11], which is essential in resolving high poloidal mode number m components in high q simulations.

The reminder of the paper is organized as follows. In Sec.2, calculation models and simulation parameters are presented. In Sec.3, the rotation scan numerical experiments are presented, and influences of toroidal rotation on E_r and heat transport are shown. In Sec.4, the q scan numerical experiments are shown, and the q dependence of heat and momentum transport is discussed. Finally, a summary is given in Sec.5.

2 Calculation models and parameters

We consider the electrostatic ITG turbulence described by gyrokinetic ions and adiabatic electrons in an axisymmetric toroidal configuration. GT5D is based on the modern gyrokinetic theory [12], in which the gyrokinetic equation system is simply given using the gyro-center Hamiltonian $H = m_i v_\parallel^2/2 + \mu B + e\langle\phi\rangle_\alpha$ and the Poisson bracket operator in the gyro-center coordinates $\mathbf{Z} = (t \in \mathbf{R}, \mathbf{v}_\parallel, \mu, \alpha)$,

$$\frac{\partial f}{\partial t} + \{f, H\} = C(f) + S_{src} + S_{snk}, \tag{1}$$

$$-\nabla_\perp \cdot \frac{\rho_{ti}^2}{\lambda_{Di}^2}\nabla_\perp \phi + \frac{1}{\lambda_{De}^2}\left(\phi - \langle\phi\rangle_f\right) = 4\pi e\left[\int f\delta([\mathbf{R}+\rho]-\mathbf{x})d^6Z - n_{0e}\right]. \tag{2}$$

Here, $\mathbf{R}$ is a position of the guiding center, $\mathbf{R}+\rho$ is a particle position, $v_\parallel$ is the parallel velocity, μ is the magnetic moment, α is the gyro-phase angle, $d^6Z = m_i^2 B_\parallel^* d\mathbf{R} dv_\parallel d\mu d\alpha$ is the phase space volume of the gyro-center coordinates, ρ_{ti} is the Larmor radius evaluated with the thermal velocity v_{ti}, λ_{Di} and λ_{De} are the ion and electron Debye lengths, ϕ is the electrostatic potential, and $\langle\cdot\rangle_\alpha$, $\langle\cdot\rangle_f$ are the gyro-average and flux-surface-average operators, respectively. The ion-ion collision operator $C(f)$ is modelled by the linear

Fokker-Planck collision operator. Source and sink terms are given as

$$S_{src} = A_{src}(\mathbf{R})\tau_{src}^{-1}\left(c_1[f_{M1} - f_{M2}] + c_2[f_{M1} - f_{M3}]\right), \quad (3)$$

$$S_{snk} = A_{snk}(\mathbf{R})\tau_{snk}^{-1}(f_0 - f), \quad (4)$$

where A_{src} and A_{snk} are deposition profiles, τ_{src} and τ_{snk} are time constants, f_{M1}, f_{M2}, and f_{M3} are shifted Maxwellian distributions, c_1 and c_2 are coefficients of power and momentum input terms, and f_0 is the initial distribution. In Eq.(3), A_{src} is localized near the axis modelling on-axis momentum and power inputs, and $f_{M1}, f_{M2}, f_{M3}, c_1, c_2$ and τ_{src} are chosen to fix input torque and power, F_{in} and P_{in}, without particle input, $\int S_{src}d^6Z = 0, \int m_i v_\parallel S_{src}d^6Z = F_{in}, \int(\frac{1}{2}m_i v_\parallel^2 + \mu B)S_{src}d^6Z = P_{in}$. In Eq.(4), T_i and $U_\parallel$ in a boundary region are modified towards their initial values by a Krook operator with the time constant τ_{snk}. This is a simple model for a boundary region in H-mode plasmas, where the pedestal temperature is limited by edge localized modes and a no-slip boundary $U_\parallel = 0$ is imposed by the charge exchange with the neutrals.

The accuracy of collisionless turbulent dynamics of GT5D was verified through linear and nonlinear ITG benchmark tests against a gyrokinetic δf particle code GT3D [9]. On the other hand, the neoclassical physics was tested in benchmark calculations against a neoclassical δf particle code FORTEC-3D [13]. Through the neoclassical benchmark, we confirmed that in the axisymmetric limit, the radial electric field is determined to satisfy a force balance relation in the local neoclassical theory [14],

$$\left\langle U_\parallel \right\rangle_f = \frac{T_i I}{m_i \Omega_i}\left(\frac{d\psi}{dr}\right)^{-1}\left[(k-1)\frac{d\ln T_i}{dr} - \frac{d\ln n_i}{dr} + \frac{e}{T_i}E_r\right], \quad (5)$$

where ψ is the poloidal flux, $I = RB_\zeta$, n_i is the ion density, and k is a coefficient of the neoclassical poloidal flow. The force balance relation was confirmed also in ITG turbulence simulations [10], where E_r is close to neoclassical levels given by Eq.(5) and keeps a balance with $U_\parallel$ determined by the turbulent momentum transport.

In the present study, we use a circular concentric tokamak configuration with $R_0/a = 2.79$, $a/\rho_{ti} = \rho^{*-1} \sim 150$, 1/3 wedge torus, and $q(r) = 0.85 + 2.18(r/a)^2$, which gives so called Cyclone like parameters, $r_s/R_0 \sim 0.18$, $q(r_s) \sim 1.4$, and $\hat{s}(r_s) = [(r/q)dq/dr]_{r=r_s} \sim 0.78$ at $r_s = 0.5a$, where R_0 is the major radius, a is the minor radius, and $q(r)$ is the safety factor. In the initial condition, plasma parameters at $r = r_s$ are given as $n_e = n_i \sim 5 \times 10^{19}\mathrm{m}^{-3}$, $T_e \sim T_i \sim 2\mathrm{keV}$, $R_0/L_n = 2.22$, $R_0/L_{te} = 6.92$, $R_0/L_{ti} = 10.0$, and $\nu^* \sim 0.025$, where $L_n = |n_i/(dn_i/dr)|$, $L_{ti} = |T_i/(dT_i/dr)|$, and ν^* is the normalized collisionality. The initial ion temperature profile is set to be far above linear and nonlinear thresholds at $R_0/L_{ti} \sim 4.5$ and at $R_0/L_{ti} \sim 6$, respectively [9, 10]. This leads to strong excitation of linear ITG modes followed by initial transient bursts, which quickly adjust temperature profiles towards a nonlinear marginal state where a power balance between source and sink is established. Power input is set as $P_{in} = 2\mathrm{MW}$ (which may be compared with the stored energy $\sim 0.245\mathrm{MJ}$ in the Zero case). Momentum input is given as $F_{in} = 0, \pm 4\mathrm{Nm}$ corresponding to zero (Zero), co-current (Co), and counter-current (Ctr) momentum input cases. Sink parameters are given as $\tau_{snk} \sim 0.1 v_{ti}/a$, $U_\parallel|_{r=a} = 0$, and $T_i|_{r=a} = 0.8\mathrm{keV}$. The source A_{src} is imposed for $r/a = 0 \sim 0.5$, while the sink is localized at $r/a > 0.9$. In between these regions, there is a source free region, where non-local avalanche like heat transport is active. Numerical parameters are chosen based on the previous work [10], except for the maximum $v_\parallel$ and the simulation duration. The former is extended to $v_\parallel = -6v_{ti} \sim 6v_{ti}$ in order to cover shifted velocity distributions induced by momentum input. The latter is enhanced to $tv_{ti}/R_0 = 0 \sim 1200$, which

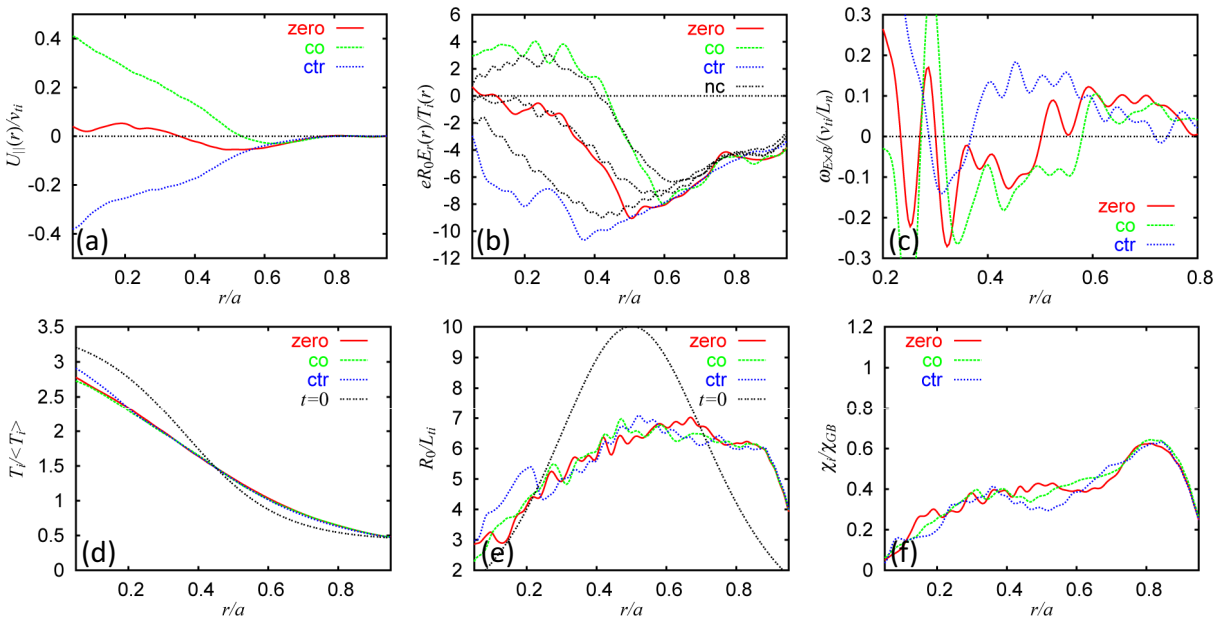

Figure 1: *The radial profiles of (a) parallel flow $U_{\parallel}$, (b) radial electric field E_r, (c) $E\times B$ shearing rate $\omega_{E\times B}$, (d) ion temperature T_i, (e) temperature gradient parameter R_0/L_{ti}, and (f) ion heat diffusivity χ_i/χ_{GB} observed in the rotation scan numerical experiments. (c),(e) and (f) are time average over the quasi-steady phase for $tv_{ti}/R_0 = 200 \sim 1200$, while (a), (b), and (d) are profiles in the final phase for $tv_{ti}/R_0 = 1060 \sim 1200$. In (b), black dashed curves show estimations using the force balance relation, Eq. (5), and profiles observed in each case. In (d), $\langle T_i\rangle$ denotes the volume average temperature at $t = 0$. In (f), χ_i is normalized by $\chi_{GB} = v_{ti}\rho_{ti}^2/L_n$.*

corresponds to about two collision times, to have better statistics of turbulent transport affected by slowly varying rotation profiles.

3 Rotation scan numerical experiments

In the rotation scan numerical experiments, the initial rotation profile is given as $U_{\parallel} \sim 0$, and rotation profiles build up due to co- and counter-current momentum inputs and non-diffusive momentum transport from a plasma boundary. Fig.1(a) shows toroidal rotation profiles. In the Zero case, an intrinsic rotation profile shows co-current toroidal rotation in the core ($r/a < 0.3$), while a notch structure of counter-current toroidal rotation is produced at $r/a \sim 0.6$. The Co and Ctr cases show formations of co- and counter-current toroidal rotation profiles due to momentum input. The parallel velocity shear rate $\gamma_p/(v_{ti}/a) = |dU_{\parallel}/dr|/(v_{ti}/a)$ at $r/a \sim 0.4$ is 0.87, 0.46, and 0.65 in the Co, Zero, and Ctr cases, respectively, while the parallel shear destabilization becomes significant for $\gamma_p > v_{ti}/a$ [3]. Therefore, its destabilizing effect seems to be irrelevant in the present rotation scan numerical experiments. It is noted that the rotation profiles in the Co and Ctr cases are not reached at the steady state, and the rotation profiles in the outer region ($r/a > 0.6$) is still similar among three cases. In contrast to the ion temperature profile which shows strong stiffness and quick relaxation towards a marginal state, the rotation profile is less stiff because it is not a main driving mechanism of the ITG turbulence. Since E_r follows the force balance relation, these rotation profiles affect mean E_r profiles in Fig.1(b). The

corresponding $E \times B$ shearing rates $\omega_{E\times B} = (r/qB)d/dr(qE_r/r)$ are shown in Fig.1(c). In the simulation, E_r consists mainly of a steady neoclassical component, a steady zonal flow component, and a dynamic avalanche component, and in Figs.1(b) and 1(c), the latter component is eliminated by the time average. The steady zonal flow component is pronounced in a core region, while in the outer region, E_r profiles are close to neoclassical levels, which typically show a global V-shape as shown in Fig.1(b). Depending on the $U_\parallel$ profile, the position of $\omega_{E\times B} = 0$ or the minimum E_r is shifted, and the sign of $\omega_{E\times B}$ is changed across this position. However, its absolute value, which is comparable to the linear growth rate $\omega_{E\times B} \sim \gamma_L$ ($\gamma_L \sim 0.11 v_{ti}/L_n$ for $R_0/L_{ti} = 6.92$), is not so different among three cases. The radial average data $\langle|\omega_{E\times B}|\rangle_r/(v_{ti}/L_n)$ is estimated as 0.066, 0.061, and 0.072 in the Co, Zero, and Ctr cases, respectively. Here, $\langle\cdot\rangle_r$ denotes the radial average over $r/a = 0.4 \sim 0.9$. In Fig.1(f), the ion heat diffusivity χ_i shows local variations reflecting the $\omega_{E\times B}$ profile, and the transport is slightly enhanced near $\omega_{E\times B} = 0$. However, global transport levels are similar among three cases, and $\langle\chi_i/\chi_{GB}\rangle_r$ is given as 0.48, 0.47, and 0.45 in the Co, Zero, and Ctr cases, respectively. As a result, T_i and R_0/L_{ti} in Figs.1(d) and 1(e) show similar profiles, and $\langle R_0/L_{ti}\rangle_r$ is respectively 6.36, 6.39, and 6.35 in the Co, Zero, and Ctr cases. According to the above data, an impact of the $U_\parallel$ profile on χ_i is not clear in the present numerical experiments. In the simulation, the momentum transport is analyzed at $r/a = 0.4$, where the momentum gradient develops sufficiently and influences from the source is relatively weak. The effective parallel momentum diffusivity $\chi_\parallel/\chi_{GB}$ averaged over $tv_{ti}/R_0 = 200 \sim 1200$ is respectively 0.25, -0.025, and 0.24 in the Co, Zero, and Ctr cases, while χ_i/χ_{GB} is 0.38, 0.39, and 0.36 at the same reference surface. From this data, effective Prandtl numbers are estimated as 0.67, -0.066, and 0.66. It is noted that a negative $\chi_\parallel$ in the Zero case shows non-diffusive momentum transport producing an intrinsic rotation. Since the Zero case develops towards a null momentum flux state, $\chi_\parallel$ becomes smaller as longer time average is applied. Since the Zero case shows an order of magnitude smaller $\chi_\parallel$ than the Co and Ctr cases, the Zero case is rather close to such a null momentum flux state.

4 Safety factor scan numerical experiments

In the q scan numerical experiments, the q profile is scaled by multiplying a constant factor of 1.2, 1.5, and 2, which are referred to as the $q \times 1.2, 1.5$, and 2 cases. This manipulation keeps the magnetic shear $\hat{s}$ unchanged. Standard parameters are given by the Zero case (the $q\times 1$ case), and the same parameters are used in the scan except for the q profile and the density. Since the neoclassical ion heat diffusivity χ_{NC} is proportional to q^2, the density is scaled to keep almost constant χ_{NC}, which is less than $\sim 0.1\chi_{GB}$ in all the cases. The collisionality is varied in the banana regime, and its influence on the poloidal flow or k in Eq.(5) is small. Figure 2 shows radial profiles observed in the q scan numerical experiments. A remarkable feature in the data is the strong q dependence of χ_i in Fig.2(f). $\langle\chi_i/\chi_{GB}\rangle_r$ is estimated as 0.47, 0.67, 0.79, and 0.84 in the $q\times 1, 1.2, 1.5$, and 2 cases, respectively. In Fig.2(d), the corresponding T_i profiles are also showing significant variations, and the core ion temperature is decreased by $\sim 24\%$ between the $q\times 1$ and 2 cases. In Fig.2(e), $\langle R_0/L_{ti}\rangle_r$ is estimated as 6.38, 6.01, 5.89, and 5.68 in the $q\times 1, 1.2, 1.5$, and 2 cases, respectively. The q dependence of turbulent transport is observed not only in the heat transport but also in the momentum transport. In Ref. [10], it was shown that the non-diffusive momentum flux shows a clear correlation against the E_r shear, and the flux is inward (outward) in the negative (positive) E_r shear region, leading to co-

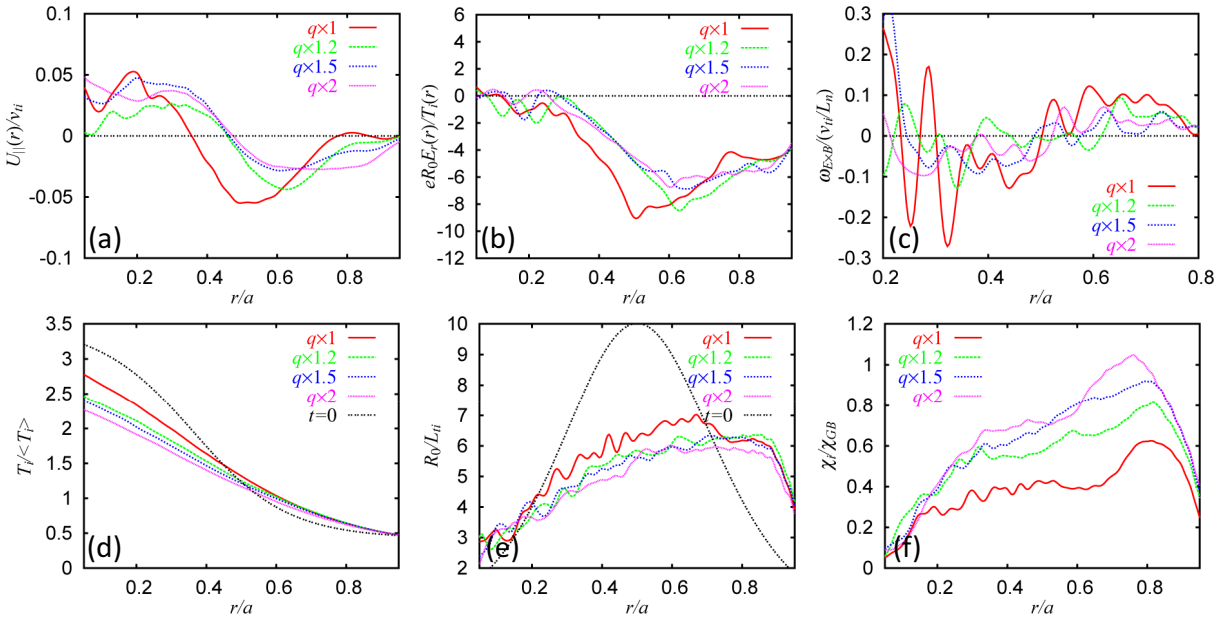

Figure 2: *The radial profiles of (a) parallel flow $U_\parallel$, (b) radial electric field E_r, (c) $E \times B$ shearing rates $\omega_{E\times B}$, (d) ion temperature T_i, (e) temperature gradient parameter R_0/L_{ti}, and (f) ion heat diffusivity χ_i/χ_{GB} observed in the safety factor scan numerical experiments. The definitions of normalization and time average are the same as Fig.1.*

current intrinsic rotation in the plasma core. The $k_\parallel$ spectra observed show opposite shifts depending on the sign of E_r shear, suggesting the existence of E_r shear stress [15]. This feature is more pronounced in the higher q cases because of higher turbulent activities. In Fig.2(a), the region of co-current toroidal rotation is enhanced from $r/a = 0 \sim 0.35$ to $r/a = 0 \sim 0.48$, and notch structures are shifted outward as in the Co case of the rotation scan numerical experiment. The time average ($tv_{ti}/R_0 = 200 \sim 1200$) of the parallel momentum flux $\Pi/(\chi_{GB} v_{ti}/a)$ at $r/a = 0.4$ is observed as -0.009, -0.047, -0.090, and -0.13 in the $q \times 1, 1.2, 1.5$, and 2 cases. It should be noted that because of stronger non-diffusive transport, rotation profiles in the higher q cases are not fully developed at $tv_{ti}/R_0 \sim 1200$, and therefore, we show Π instead of $\chi_\parallel$. The resulting $U_\parallel$ profiles lead to weaker E_r shear in Fig.2(b), and in Fig.2(c), $\langle|\omega_{E\times B}|\rangle_r$ is respectively estimated as 0.061, 0.027, 0.030, and 0.032 in the $q \times 1, 1.2, 1.5$, and 2 cases.

In order to understand the mechanism of enhanced turbulent transport, the simulation results are studied form the viewpoints of turbulent correlation time and length $(\Delta t v_{ti}/a, \Delta r/\rho_{ti})$, geodesic acoustic mode (GAM) activities, and $E \times B$ shearing suppression of linear ITG modes. $(\Delta t v_{ti}/a, \Delta r/\rho_{ti})$ estimated for $n \neq 0$ components of ϕ at the outboard mid plane is (2.1,4.3), (2.3,5.0), (2.2,5.1), and (2.4,4.9) in the $q \times 1, 1.2, 1.5$, and 2 cases. Although early linear theory [7] predicted $\Delta r \propto q^{1/2}$ and a similar dependence is used in several quasi-linear models [3], the above correlation analysis does not support such q dependency. Another mechanism found in recent simulation studies [8] is the q dependence of GAM activities, which interfere suppression of turbulent transport due to generation of static zonal flows. In Fig.3(b), GAM oscillations are normally observed in the initial GAM damping phase, and their frequencies and damping rates agree well with theory [13], which shows the q dependence of the damping rate. In Fig.3(c), such GAM oscillations are observed also in the transient bursty phase of the $q \times 2$ case. However, in

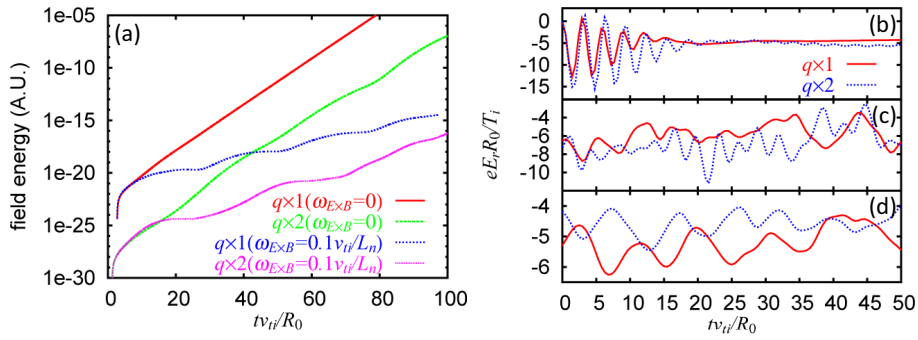

Figure 3: *Comparisons of the $q\times1$ and $q\times2$ cases. (a) The linear growth of ITG modes with and without the E_r shear with $R_0/L_{ti}=6.92$ and $\Omega_{E\times B}=0.1v_{ti}/L_n$. (b), (c), and (d) shows time histories of E_r at $r/a=0.7$ ($q=1.92$ and 3.84) observed in (b) initial GAM damping phase, (c) transient bursty phase, and (d) quasi-steady phase.*

Fig.3(d), GAM activities are not observed in the quasi-steady phase, and both the $q\times1$ and 2 cases show similar slow variations of E_r, which are in a force balance state with avalanches of the temperature gradient [10]. Therefore, a role of GAMs is not clear in our q scan numerical experiments, which operate near marginally stable profiles. The linear calculations of most unstable toroidal modes, $n=15$ and $n=9$, in the $q\times1$ and 2 cases are shown in Fig.3(a). Without the E_r shear, both cases give comparable linear growth rates ($\gamma_L/(v_{ti}/L_n)=0.11$ and 0.10 in the $q\times1$ and 2 cases). However, with externally imposed E_r shear with $\omega_{E\times B}=0.1v_{ti}/L_n$, they give significantly different growth rates, and the E_r shear stabilization is less effective for the $q\times2$ case ($\gamma_L/(v_{ti}/L_n)=0.38$ and 0.49 in the $q\times1$ and 2 cases). In addition, in Fig.2(c), $\langle\omega_{E\times B}\rangle_r$ of the $q\times2$ case is about a half compared with the $q\times1$ case. Therefore, this linear stability mechanism is important for explaining the q dependence of the turbulent transport.

5 Summary

In this work, we have studied an impact of the toroidal rotation and the safety factor on the ITG turbulence using GT5D. In the present rotation scan numerical experiments, the mean E_r profile, which is close to neoclassical levels, is changed depending on the momentum input, while the magnitude of its shearing rate $|\omega_{E\times B}|$ is on average comparable among the Co, Zero, and Ctr cases. It is noted that even without the momentum input, the E_r profile with $|\omega_{E\times B}|\sim\gamma_L$ is sustained by the poloidal rotation, profile shear effects, and intrinsic rotation. As a result, χ_i and R_0/L_{ti} are similar among the three cases, and an impact of the toroidal rotation on the turbulent transport and the T_i profile is not clearly seen in the present rotation scan numerical experiments. The result seems to be consistent with rotation scan experiments on JT-60U [1], which did not show a clear change in R_0/L_{ti}. However, it is difficult to explain the results on JET [2], which showed significant degradation of R_0/L_{ti} with low toroidal rotation. Main differences between the former and latter rotation scan experiments are the q profile and ρ^* ($(q_{95},\rho^*)\sim(4,1/230)$ and $(6,1/560)$ on JT-60U and JET). Although the same rotation scan was repeated in the $q\times1.5$ and 2 cases, χ_i and R_0/L_{ti} did not show significant changes depending on the momentum input. On the other hand, smaller ρ^* plasmas are characterized by lower profile shear and $\omega_{E\times B}$ [16], and the effects of toroidal rotation may be more pronounced at

smaller ρ^*. In order to understand differences between JT60U and JET, further numerical experiments with realistic ρ^* and momentum input conditions are needed.

In the q scan numerical experiments, turbulent transport is significantly increased at higher q. In the simulations, the q dependence of turbulent correlation time and length is small, and GAM activities are not observed in the quasi-steady phase even at high q. In contrast to the above mechanisms reported in early works, we found that the stabilizing effect of E_r shear on linear ITG modes becomes less effective at higher q. In the q scan, both the heat and momentum transport is affected by the q profile. The higher q cases show larger χ_i and lower R_0/L_{ti}, and between the $q \times 1$ and 2 cases, χ_i is almost doubled and the core temperature is decreased by $\sim 24\%$. On the other hand, the non-diffusive inward momentum transport with the negative E_r shear is significantly increased at higher q, and a region of co-current spontaneous rotation is enhanced in the plasma core. Although the rotation profiles are not fully developed yet in the present q scan numerical experiments, these results are qualitatively consistent with the I_p dependence of the energy confinement [5] and the intrinsic rotation [6].

GT5D simulations in this work were performed on FX1 at Nagoya Univ., T2K at Univ. Tokyo, and Altix3700Bx2, BX900, FX1 at JAEA. One of the authors (Y.I.) is supported by the MEXT, Grant No.22686086.

References

[1] H. Urano, H. Takenaga, T. Fujita, *et al.*, Nucl. Fusion **48**, 085007 (2008).

[2] P. Mantica, D. Strintzi, T. Tala, *et al.*, Phys. Rev. Lett. **102**, 175002 (2009).

[3] R. Waltz, G. D. Kerbel, and J. Milovich, Phys. Plasmas **1**, 2229 (1994).

[4] A. M. Dimits, T. J. Williams, J. A. Byers, *et al.*, Phys. Rev. Lett. **77**, 71 (1996).

[5] J. G. Cordey, *et al.*, Nucl. Fusion **43**, 670 (2003).

[6] J. E. Rice, *et al.*, Nucl. Fusion **47**, 1618 (2007).

[7] W. Horton, D. Choi, and W. Tang, Phys. Fluids **24**, 1077 (1981).

[8] N. Miyato, Y. Kishimoto, and J. Li, Phys. Plasmas **11**, 5557 (2004); P. Angelino, *et al.*, Plasma Phys. Control. Fusion **48**, 557 (2006).

[9] Y. Idomura, M. Ida, T. Kano, *et al.*, Comput. Phys. Commun. **179**, 391 (2008).

[10] Y. Idomura, H. Urano, N. Aiba, *et al.*, Nucl. Fusion **49**, 065029 (2009).

[11] S. Jolliet, *et al.*, submitted to J. Comput. Phys.

[12] A. J. Brizard and T. S. Hahm, Rev. Mod. Phys. **79**, 421 (2007).

[13] S. Satake, Y. Idomura, H. Sugama, *et al.*, Comput. Phys. Commun **181**, 1069 (2010).

[14] F. L. Hinton and R. D. Hazeltine, Rev. Mod. Phys. **48**, 239 (1976).

[15] R. R. Dominguez and G. M. Steabler, Phys. Fluids B **5**, 3876 (1993); Ö. D. Gürcan, *et al.*, Phys. Plasmas **14**, 042306 (2007).

[16] S. Jolliet and Y. Idomura, THC/P4-14, this conference.